AD708015

NOLTR 70-38

ANALYTICAL AND EXPERIMENTAL STUDY OF THE DYNAMIC RESPONSE OF CABLE SYSTEMS

By
Jack E. Goeller

23 FEBRUARY 1970

NOL

UNITED STATES NAVAL ORDNANCE LABORATORY, WHITE OAK, MARYLAND

NOLTR 70-38

DDC
RECEIVED
JUL 2 1970
C

ATTENTION

This document has been approved for public release and sale, its distribution is unlimited.

43

DISCLAIMER NOTICE

THIS DOCUMENT IS BEST QUALITY PRACTICABLE. THE COPY FURNISHED TO DTIC CONTAINED A SIGNIFICANT NUMBER OF PAGES WHICH DO NOT REPRODUCE LEGIBLY.

NOLTR 70-38

ANALYTICAL AND EXPERIMENTAL STUDY OF THE DYNAMIC RESPONSE OF CABLE SYSTEMS

Prepared by:
Jack E. Goeller

ABSTRACT: Segmented cables of steel and nylon are frequently used in oceanographic applications to support a suspended payload. This report contains an experimental and analytical study of the dynamic response of nylon rope and stranded steel cables with a suspended payload under simulated conditions of ocean wave motion. A generalized distributed mass model was developed for a segmented cable made up of two viscoelastic materials, including internal damping and linear external damping of the payload and cable. Viscoelastic behavior was simulated by a two-parameter Voigt model. A three-parameter model (standard linear solid) was also studied for a discrete parameter system. Experimental tests were conducted in air and water on cables of the order of 70 feet in length and 0.25 inch in diameter. The results compared well with theory over the fundamental frequency range.

U. S. NAVAL ORDNANCE LABORATORY
WHITE OAK, MARYLAND

NOLTR 70-38 23 February 1970

ANALYTICAL AND EXPERIMENTAL STUDY OF THE DYNAMIC RESPONSE OF CABLE SYSTEMS

This effort was conducted by the Hydroballistics and Mechanics Division of the Ballistics Department for future application to buoy or moored systems. The author wishes to acknowledge the support given by Drs. P. A. Laura and M. Casarella of the Catholic University of America, and Drs. A. E. Seigel and V. C. D. Dawson of the Naval Ordnance Laboratory.

GEORGE G. BALL
Captain, USN
Commander

a.e. Seigel

A. E. SEIGEL
By direction

CONTENTS

ILLUSTRATIONS

TABLES

REFERENCES

1. Richardson, William S., "Buoy Mooring Cables, Past, Present, and Future," Transaction, 2nd International Buoy Technology Symposium, 18-20 Sep 1967, Washington, D. C., pp 15-18
2. Goeller, J. E. and Laura, P. A., "Dynamic Stress and Displacements in a Two-Material Cable System Subjected to Longitudinal Excitation," Journal of the Acoustical Society of America, Vol. 46, No. 2, (Part 1) Aug 1969
3. Wilson, B. W., "Characteristics of Anchor Cables in Uniform Ocean Currents," Texas A & M, AM Project 204, Tech. Report No. 204-1, Apr 1960
4. Reid, R. O., "Dynamics of Deep Sea Mooring Lines," Texas A & M, AM Project 204, Tech. Report No. 68-11F, Jul 1968
5. Snowden, J. C., Vibration and Shock in Damped Mechanical Systems, 1st Ed., Wiley & Sons, 1968
6. Paquette, R. G. and Henderson, B., "The Dynamics of Simple Deep Sea Buoy Mooring," G. M. Corp., Nov 1965
7. Goeller, J. E., "Theoretical and Experimental Investigation of a Flexible Cable System Subjected to Longitudinal Excitation," PhD dissertation, Catholic University of America, 1969

NOMENCLATURE

A_p	projected area of spherical payload $A_p = \frac{\pi}{4} D^2$
A	effective cross section area of homogeneous cable $A = .404\ d^2$
a	acoustic sound speed in elastic cable
C	damping coefficient
C_{CR}	critical damping ratio $C_{CR} = 2\sqrt{k_e M_e}$
C_1, C_2, C_3, C_4	complex constants
C_{DP}	drag coefficient of payload
C_{DC}	drag coefficient of cable
D	diameter of payload mass
d	diameter of cable
E	modulus of elasticity
F_4, G_4	constants defined by Eq. (B-37) of [7]
F_5, G_5	constants defined by Eq. (B-38) of [7]
f	damping constant of fluid
$G(\omega)$	complex modulus of three-parameter viscoelastic model
g	gravitational constant
K	spring constant
K_o	apparent spring constant of nylon for cyclic motion
L	length of cable
m	frequency ratio $m = \frac{\omega_t}{\omega_{ne}}$
M_e	effective mass = $M_p + M_{vm}$

M_p	mass of payload
M_{vm}	virtual mass of displaced water
P	axial force in cable
p	perimeter of cable
T	period of sinusoidal function $T = \frac{2\pi}{\omega}$
T_{STAT}	static force in cable due to payload $W_p - W_B$
t	time
U_{max}	maximum displacement of payload
u	axial displacement
W	frictional energy dissipated by damping
W_B	buoyancy force due to displaced payload
W_p	weight of payload
w	frictional energy per unit length dissipated by damping
x	spatial variable (see Figure 1)
x_o	maximum amplitude of displacement function
Y	ratio of spring constants $Y = \frac{k_2}{k_3}$
λ	complex Eigen value function ($\lambda = \alpha + i\theta$)
α	real part of λ
β	viscous damping coefficient $\beta = \frac{f\mu}{AE}$
δ	static deflection of mass
$\delta(\omega)$	damping factor depending on frequency
θ	imaginary part of λ
μ	viscosity
γ	definition $\gamma = \omega t - \phi$

ϵ	strain $\frac{\partial u}{\partial x}$
ρ	density
φ	phase angle
σ	axial stress in cable
τ	time constant of viscoelastic model
ω_{ne}	natural frequency of simple spring mass system; $\omega_{ne} = \sqrt{\frac{K_e}{M_e}}$
ω	circular frequency of forcing function
ζ	damping ratio = $\frac{C}{C_{CR}}$
Ω	frequency ratio $\frac{\omega}{\omega_{ne}}$

SUBSCRIPTS

p	payload
c	cable
e	effective
v	viscoelastic model
j	identifies segment of cable j = 2, 3

INTRODUCTION

Nylon rope and stranded steel cable are frequently used in oceanographic cable systems. Nylon is highly desirable for buoy systems, mooring systems, and other oceanographic applications because of its lightweight, relatively good strength, and ease of handling. However, in cases where fishbite is a problem [1], steel stranded cable is used in the upper portion of the cable while nylon is used in the lower portion. Many applications invo. ve the suspension of a payload by a segmented cable of steel and nylon where the upper end is excited by longitudinal oscillation due to ocean wave motion. This problem was studied analytically [2] by approximating the wave motion as a sinusoidal displacement function. The cable segments were considered as distributed masses with viscoelastic behavior including internal damping and also external damping due to fluid viscosity. The purpose of this paper is to compare experimental data with theoretical prediction, using this model and a second analytical model which approximates viscoelastic behavior of nylon rope by a three-parameter model, frequently referred to as a stranded linear solid.

MATHEMATICAL MODELS

a. Model No. 1 - Distributed Mass Voigt Model

The following is a summary of the pertinent characteristics of the first model. For a detailed discussion and derivation of equations, the reader is referred to [2]. The model is shown schematically in Figure 1. The model considers the cable as being made up of two segments of different viscoelastic materials. A two-parameter Voigt model is used for each segment. A continuum approach was used as opposed to the frequently used discrete parameter model. The viscous damping of the water was considered for both the cable and payload by assuming the damping to be linearly dependent on the local velocity. Damping forces are, in general, proportional to velocity squared, but an approximate linear damping coefficient was obtained by equating the frictional energy dissipated by linear damping to that dissipated by velocity squared damping. In order to have a generalized theoretical model, the payload was considered to be attached to a rigid foundation by an elastic spring and dashpot. This model is an approximation to the salvage recovery problem where the mass is originally settled in the ocean sediments. If the spring constant is set equal to zero, the model corresponds to a floating buoy or ship with a payload suspended from the bottom of the cable.

For each segment ($j = 2, 3$), the material is considered to behave in accordance with a constitutive relationship of the form:

$$\sigma_{xj} = E_j \frac{\partial u_j}{\partial x_j} + \mu_{vj} \frac{\partial}{\partial t}\left(\frac{\partial u_j}{\partial x_j}\right) \qquad (1)$$

where E_j is the elastic modulus and μ_{vj} is the internal viscosity coefficient. Considering linear external damping on the wetted cable, the equation of motion for each segment is

$$\frac{\partial^2 u_j}{\partial x_j^2} + \tau_j \frac{\partial^3 u_j}{\partial x_j^2 \partial t} - \beta_j \frac{\partial u_j}{\partial t} = \frac{1}{a_j^2} \frac{\partial^2 u_j}{\partial t^2} \tag{2}$$

where

$$\tau_j = \frac{\mu_{vj}}{E_j} \qquad \text{time constant of the viscoelastic model}$$

$$a_j = \sqrt{\frac{E_j}{\rho_j}} \qquad \text{sound velocity in the cable material}$$

$$\beta_j = \frac{f_j \mu_{fi}}{A_j E_j} \qquad \text{viscous damping coefficient of the fluid}$$

The steady-state solution to equation (2) for a sinusoidal displacement function, $x = x_o \sin \omega t$, is given by the complex part of the following equation

$$u_j (x_j, t) = X (x) e^{i\omega t} \qquad j = 2.3 \tag{3}$$

By following the procedures in [2], it can be shown that the solution is

$$\begin{aligned} u_2 (x_2, t) &= e^{i\omega t} (C_1 \sin \lambda_2 x_2 + C_2 \cos \lambda_2 x_2) \\ u_3 (x_3, t) &= e^{i\omega t} (C_3 \sin \lambda_3 x_3 + C_4 \cos \lambda_3 x_3) \end{aligned} \tag{4}$$

where

$$a_j = \sqrt{\frac{\left[(\frac{\omega}{a_j})^2 - \tau_j \beta_j \omega^2\right] + \sqrt{\left[(\frac{\omega}{a_j})^2 - \tau_j \beta_j \omega^2\right]^2 + \left[\beta_j \omega + \tau_j \omega (\frac{\omega}{a_j})^2\right]^2}}{2(1 + \tau_j^2 \omega^2)}}$$

$$\theta_j = \sqrt{\frac{-\left[\left(\frac{\omega}{a_j}\right)^2 - \tau_j \beta_j \omega^2\right] + \sqrt{\left[\left(\frac{\omega}{a_j}\right)^2 - \tau_j \beta_j \omega^2\right]^2 + \left[\beta_j \omega + \tau_j \omega \left(\frac{\omega}{a_j}\right)^2\right]^2}}{2(1 + \tau_j^2 \omega^2)}}$$

The constants C_1, C_2, C_3, and C_4 are determined from the following four boundary conditions:

$$u_3 (L_3, t) = x_o e^{i\omega t} \tag{5}$$

$$\sigma_{x2} A_2 = M_e \left(\frac{\partial^2 u_2}{\partial t}\right)_{x_2 = 0} + C_p \left(\frac{\partial u_2}{\partial t}\right)_{x_2 = 0} + K_s (u_2)_{x_2 = 0} \tag{6}$$

$$u_2 (L_2, t) = u_3 (0, t) \tag{7}$$

$$A_2 \left[E_2 \frac{\partial u_2}{\partial x_2} + \mu_{v2} \frac{\partial}{\partial t} \left(\frac{\partial u_2}{\partial x_2}\right)\right]_{x_2 = L_2} = A_3 \left[E_3 \frac{\partial u_3}{\partial x_3} + \mu_{v3} \frac{\partial}{\partial t} \left(\frac{\partial u_3}{\partial x_3}\right)\right]_{x_3 = 0} \tag{8}$$

The "effective mass M_e" includes the payload mass and the virtual mass of displaced water. The first boundary condition is the prescribed displacement at the upper end. The second is obtained from a force balance at the payload. The third and fourth require compatibility of displacement and force at the joint between the cable segments. The results obtained were expressed in terms of the natural frequency ω_{ne} of a massless cable system using the equivalent spring constant

$$K_e = \frac{K_2 K_3}{K_2 + K_3}$$

The following expressions were obtained for the dimensionless force in the cable segments

$$\frac{P_2}{K_e x_o} = \frac{1 + Y}{x_o} \left\{(F_4 - \tau_2 \omega G_4) \sin\omega t + (G_4 + \tau_2 \omega F_4) \cos\omega t\right\} \tag{9}$$

$$\frac{P_3}{K_e x_o} = \frac{1 + Y}{Y x_o} \left\{ (F_5 - \tau_3 \omega G_5) \sin\omega t + (G_5 + \tau_3 \omega F_5) \cos\omega t \right\} \tag{10}$$

where F_4, F_5, G_4, and G_5 are lengthy transcendental functions dependent on the position coordinates x_2 and x_3. In order to obtain these values an 8 x 8 matrix must be solved. The details of this solution are given in Ref. 2 . Equations (9) and (10) give the dynamic force in the cable. The total cable force can be obtained by adding the static force due to the payload and cable weight. The solution given is valid provided the total cable force is always tensile since the cable cannot support a compressive stress.

The damping coefficients C_p and $f_j \mu_j$ can be estimated by equating the energy dissipated for linear damping to that dissipated by velocity squared damping. Following this approach it is shown in Appendix A that

$$C_p = \frac{4}{3\pi} \rho C_{DP} A_p U_{max} \omega \tag{11}$$

and

$$(f\mu)_{Aver} = \frac{4 \rho C_{DC} \omega d}{3} \left\{ \frac{U_{max}^3 - \frac{3}{2} U_{max}^2 (U_{max} - x_o)}{U_{max}^2 - U_{max} (U_{max} - x_o) + \frac{(U_{max} - x_o)^3}{3}} + \frac{U_{max} (U_{max} - x_o)^2 - \frac{1}{4} (U_{max} - x_o)^3}{U_{max}^2 - U_{max} (U_{max} - x_o) + \frac{(U_{max} - x_o)^3}{3}} \right\} \tag{12}$$

where

$$C_{DP} = \frac{F_D}{\frac{1}{2} \rho A_p V^2}$$

$$C_{DC} = \frac{F_c}{\frac{\pi}{2} \rho d V^2}$$

Estimates of C_{DC} for standard steel cable can be obtained from [3].

The internal damping "time constant τ" of the nylon was obtained from experimental free oscillation tests.

b. Model No. 2 - Three-Parameter Discrete Model

The main disadvantage of Model No. 1 is that the spring constant is considered to be a constant, whereas in real viscoelastic materials both the spring constant and the internal damping factor are dependent on frequency. In order to investigate the effect of frequency, a three-parameter model as shown in Figure 2 was examined. The characteristic behavior of this model is useful in explaining the experimental behavior observed in nylon ropes. For example, the constitutive relation in terms of force-strain is:

$$\left(K_2 + \mu \frac{\partial}{\partial t}\right) P = \left(K_1 K_2 + (K_1 + K_2) \mu \frac{\partial}{\partial t}\right) \epsilon \qquad (14)$$

From the theory of linear viscoelasticity, the substitution of $(i\omega)^n$ for $\frac{\partial^n}{\partial t^n}$ is permissible. This yields

$$\frac{\sigma}{\epsilon} = \frac{L}{A}\left[\frac{K_1 K_2 + \mu^2 \omega^2 \left(K_1 + K_2\right) + i\mu\omega K_2^2}{K_2^2 + \mu^2 \omega^2}\right] = G(\omega) \qquad (15)$$

The real part is frequently referred to as the storage modulus and the imaginary part as the loss modulus. If we apply a harmonic force of the form

$$P = P_{STAT} + \Delta P \cos \omega t$$

Then a plot of P versus ϵ can be made [4] as shown in Figure 3 using equation (14). The slope of the diagonal A-B can be interpreted as an "apparent dynamic spring constant." Thus the apparent spring constant is frequency dependent. Moreover, for low frequency it approaches the static spring constant and at high frequency it approaches $(K_1 + K_2)$. The "apparent spring constant K_o" at resonance can be estimated from natural frequency measurements by $K_o = M_e \omega_{ne}^2$. This will be higher than the static spring constant. This was found to be true in the experiments where the static spring constant was found to be about 2.9 lb/in compared to the estimated apparent spring constant of 3.4 lb/in. The damping factor $\delta(\omega)$, which is a measure of the mechanical loss in the system, is given by

$$\delta(\omega) = \frac{\mu \omega K_2^2}{K_1 K_2^2 + \mu^2 \omega^2 (K_1 + K_2)} \qquad (16)$$

It has a maximum value at a frequency called the transition frequency [5]. This can be obtained by

$$\frac{d\,\delta(\omega)}{d\,\omega} = 0 \tag{17}$$

Hence, we obtain

$$\omega_t = \frac{K_2}{\mu\,\alpha^{1/2}}$$

where α is the ratio of the high to low spring constant; namely, $\frac{K_1 + K_2}{K_1}$. The corresponding maximum value of $\delta(\omega)$ is

$$\delta_{max} = \frac{\alpha - 1}{2\sqrt{\alpha}} \tag{18}$$

For damping less than 0.3, δ_{max} is approximately equal to $1/\pi$ times the logarithmic decrement [5] and is equivalent to $\tau\omega_{ne}$ which is used in Model No. 1. This was measured in the free oscillation air tests and was found to be .158 for 1/4-inch nylon. Knowing δ_{max}, the quantity α can be computed from equation (18) viz

$$\alpha = 1 + 2\,\delta_{max} + \left(1 + \delta_{max}^2\right)^{1/2} + 2\,\delta_{max}^2 \tag{19}$$

The equation of motion in terms of the complex modulus $G(\omega)$ is

$$M_e \frac{d^2 x_2}{dt^2} + C_p \frac{d\,x_2}{dt} = G(\omega)\,(x_1 - x_2) \tag{20}$$

where

$$x_1 = x_o\, e^{i\omega t} \tag{21}$$

The solution exists in the form

$$x_2 = X^*\, e^{i\omega t} \tag{22}$$

The complex modulus can be written as

$$G(\omega) = K(\omega)\,[1 + i\,\delta(\omega)] \tag{23}$$

Utilizing equation (20), equation (21), equation (22), and equation (23) it can be shown that:

$$\frac{X^*}{x_o} = \frac{\sqrt{1 + \delta(\omega)^2}}{\sqrt{\left(1 - \frac{Me\,\omega^2}{K(\omega)}\right)^2 + \left(\frac{C_p\,\omega}{K(\omega)} + \delta(\omega)\right)^2}} \tag{24}$$

If $K(\omega) = K_o$ at the natural frequency ω_{ne} of the system

$$\omega_{ne}^2 = \frac{K_o}{M_e}$$

Then it can be shown that

$$\frac{K_o}{K(\omega)} = \frac{(\Omega^2 + m^2\,\alpha)\,(1 + m^2)}{(\Omega^2 + m^2)\,(1 + m^2\,\alpha)} \tag{25}$$

$$\delta(\omega) = \frac{2\,\Omega\,m\,\delta_{max}}{\Omega^2 + m^2} \tag{26}$$

where

$$\Omega = \frac{\omega}{\omega_{ne}} \text{ and } m = \frac{\omega_t}{\omega_{ne}}$$

We can now write equation (24) as

$$\frac{X^*}{x_o} = \frac{\sqrt{(\Omega^2 + m^2)^2 + (2\,\Omega\,m\,\delta_{max})^2}}{\sqrt{Q^2 + S^2}} \tag{27}$$

where

$$Q = \Omega^2 + m^2 - \frac{\Omega^2\,(\Omega^2 + m^2\,\alpha)\,(1 + m^2)}{1 + \alpha\,m^2}$$

$$S = \frac{2\,\zeta_p\,\Omega\,(\Omega^2 + m^2\,\alpha)\,(1 + m^2)}{1 + \alpha\,m^2} + 2\,m\,\Omega\,\delta_{max}$$

The force in the cable can best be obtained from

$$P = (-M_e X^* \omega^2 + C_p X^* \omega i)\, e^{i\omega t}$$

The maximum cable force is

$$P_{max} = K_o x_o \sqrt{\left(\frac{\omega}{\omega_{ne}}\right)^4 + \left(2 \zeta_p \frac{\omega}{\omega_{ne}}\right)^2} \frac{X^*}{x_o} \qquad (28)$$

In these equations, it is reasonable to assume that the transition frequency is identical to the natural frequency. Hence, m was taken equal to 1.

TEST APPARATUS

The tests were performed at the Naval Ordnance Laboratory using the Hydroballistics Tank shown in Figure 4. The tank is approximately 35 feet wide by 100 feet long with a water level of up to 65 feet. The water is of high purity. The driving mechanism for oscillating the cable was located on the top deck with the cable inserted through a porthole in the deck. A portion of the cable length was in air while the major portion was immersed in the water. The payload could be photographed through ports in the sides of the tank.

The driving mechanism for oscillating the cable is shown in Figure 5. It is essentially a crank-type device with a drive rod attached to the flywheel. The prime mover consisted of a d-c shunt electric motor with a reduction gear for reducing the speed and increasing the torque capability. The motor had adjustable speed, but at a given setting the speed was insensitive to changes in the applied torque.

The force in the cable specimens was measured by load cells located at top and bottom of the cable. The load cell used was model A 8293 as manufactured by Schaevitz with a maximum load capability of 1000 pounds. The voltage output was fed to a Beckman-type R oscillograph where a trace of force versus time was obtained. Prior to each test, the instrumentation was calibrated by applying known weights to the load cells.

The payload was a sphere of 8-inch diameter which was made of solid aluminum with a weight of 26.9 pounds, including attachment fittings. The weight of the sphere in water is 17.8 pounds, excluding the weight of the attached cable. The virtual mass, or added mass, of the displaced water is 0.15 slugs (4.85 pounds).

Tests were performed on segmented cables of steel and nylon, and cables of nylon alone. Pertinent characteristics of the cables

are given in Table 1. The steel can best be described as aircraft-type cables constructed of carbon steel according to MIL-W-1511. The diameter was 3/16 inch with 7 wires per strand and 19 strands per cable. The nylon rope was 1/4 inch diameter and can best be described as a braided rope with a breaking strength of 1150 pounds. Experimental static force-elongation data for a 73-foot length of nylon rope are shown in Figure 6. The data shown are for the loading phase. The nylon rope exhibited appreciable hysteresis during unloading. The force-elongation data also depends on previous history. For example, curve A is for the first test. Curve B is for the last of the three succeeding tests. The rope exhibited an increase in stiffness for the latter test. Dynamic force-elongation data on 1/2-inch nylon rope from [6] also indicated a hysteresis loop. The data also show that the apparent spring constant (slope of the principal axis of the hysteresis loop) increases with increasing mean load. It was also observed that the apparent spring constant under dynamic cyclic load is higher than the static spring constant. This fact makes the static spring constant rather useless in predicting dynamic response of oscillating cable systems. It was also shown that the dynamic spring constant for 1/4-inch nylon rope is significantly higher than the static spring constant obtained from Figure 6. The apparent spring constant for cyclic operation was estimated from measurements of the system natural frequency, i.e., $K_e = M_e \omega_{ne}^2$. It was also shown that K_e is significantly lower in water compared to air.

EXPERIMENTAL RESULTS

a. Nylon Rope Tests in Air (System No. 1)

Forced oscillation tests were performed on 1/4-inch nylon rope 73 feet long with the 8-inch diameter spherical payload. The tests were performed in both air and water. The tests were performed in air for several reasons. The first was to estimate the internal damping of the cable free of any external damping. Secondly, it was desired to observe the pulse shapes in air so that the effect of the water in causing nonlinearities could be observed. Thirdly, it is a known fact that the elastic properties of nylon change when exposed to water. This then would have an effect on the natural frequencies and the cable force.

The system was oscillated at the top at displacement amplitudes of one to three inches. The forcing frequency range was zero to three Hz. Typical oscillograph traces are shown in Figure 7. The response is very nearly sinusoidal and was found to be very reproducible. Similar response traces were obtained at displacement amplitudes of up to three inches. Beyond this displacement amplitude, snap loads due to slack in the cable become very pronounced. For a discussion of snap loads in cable the reader is referred to [7].

TABLE 1

CHARACTERISTICS OF CABLE TEST SPECIMENS

System No. -	Mat'l -	Dia Inch	Length Ft	No. of Strands -	Wt 100 Ft lbs	Dry Wt lbs	Spring Const Air lb/in	Spring Const Water lb/in	Natural Freq Air Hz	Natural Freq Water Hz	Break Str lbs
1	Nylon	1/4	73	Braided	1.66	1.21	3.1 to 3.8	1.7	1.06 to 1.18	.72	1150
2	St'l	3/16	36.5	7 x 19	6.5	2.37	7.35	3.7	1.59	1.05	1150
	Nylon	1/4	34.5	Braided	1.66	.57					
3	St'l	3/32	62	7 x 7	1.60	.99	28	16.8	3.16	2.28	920
	Nylon	1/4	6	Braided	1.60	.099					

Natural Freq Based on Wt of Payload + Virtual Mass + 1/3 Cable Wt

26.9 lbs + 4.85 lbs + 1/3 W_{cable} (lbs)

In order to effectively get a comparison between the theory formulated by Model No. 1 and Model No. 2 and experiment, the experimental data were non-dimensionalized by plotting $\frac{P}{K_e X_o}$ versus $\frac{\omega}{\omega_{ne}}$. The dynamic component P was obtained by subtracting the static force "T_{STAT}" from the maximum cable force. The natural frequency was considered as the value of ω_{ne} for which the displacement of the mass, in the absence of damping, becomes infinitely large as a function of time. An approximation was obtained as the frequency which causes resonance. Verification was obtained from the free oscillation tests. For the nylon rope specimen, it was found to range from 1.06 Hz to 1.18 Hz. The apparent dynamic spring constant was computed from the natural frequency, i.e., $K_e = M_e \omega_{ne}^2$. The internal damping factor of $\tau\omega_{ne} = 0.158$ was obtained from Figure 8 which is the force-time response of a free oscillation test. It can be shown that $\tau\omega_{ne}$ is approximately equal to $1/\pi$ times the logarithmic decrement. Using these values, the computed dimensionless cable force was compared to experimental results as shown in Figure 9. The comparison is reasonably good for frequency ratios up to resonance. The experimental results are slightly lower in the low frequency range, but this is probably due to the nonlinear characteristics of the cable. The steeper rise near resonance is very close to a jump condition. The good agreement was probably obtained because of the relatively small elongation of the cable resulting in near linear behavior. At higher frequencies the experimental results are somewhat higher than the distributed mass model. Also the experimental results show a dependency on excitation amplitude, whereas the theoretical force ratio $\frac{P}{K_e x_o}$ plots as a line independent of excitation amplitudes. The dependency on amplitude was also observed in the water tests.

It was hoped that better agreement between theory and experiment could be obtained by a mathematical model which accounts for increase in stiffness with frequency. The three-parameter Model No. 2 has this characteristic plus the characteristics of damping dependency on frequency. The internal damping reaches a maximum at the transition frequency, then continues to decrease. It was assumed that this transition frequency occurs at the natural frequency viz m = 1. Figure 10 shows a plot of equation (28) compared to the distributed mass-Voigt Model No. 1 and the average of the experimental data. The three-parameter Model No 2 shows slight improvement at the higher frequency. The improvement was not as good as expected because the damping factor decreases at the high frequency range, whereas in many materials it actually increases with frequency. Hence, it is believed that better

agreement could be obtained if the material properties are obtained in a dynamic test as a function of frequency and these properties are used in combination with the distributed mass model.

b. Nylon Rope Tests in Water (Specimen No. 1)

Forced oscillation tests were performed in water on 1/4-inch rope 73 feet long with the 8-inch spherical payload. The system was oscillated at the top at displacement amplitudes of one to four inches. Typical force-time response plots are shown in Figure 11. At low frequency a nonlinear response was observed which was not observed in the air tests. The nonlinearity is probably caused by the damping of the water. At higher frequency the effect of nonlinearity disappears and the response is very nearly sinusoidal.

Free oscillation tests were also performed in water to estimate the damped natural frequency. It was found that the average natural frequency in water was about .72 Hz compared to an average 1.10 Hz in air. This indicates a significant lower spring constant in water.

The experimental data were non-dimensionalized by estimating the spring constant from measurements of the natural frequency. Figure 12 shows the comparison between experiment and theory using the distributed mass Model No. 1. The tangential drag coefficient per unit length of cable C_{DC} was estimated to be .010 from Figure 5-15 of [3]. The plot of C_{DC} is relatively constant beyond a Reynolds number of 500. The Reynolds number for 0.25-inch nylon rope at a velocity of 1 ft/sec is about 2000 and is therefore greater than 500 over the major portion of a cycle of oscillation. The assumption of constant drag coefficient then appears reasonable. In general, the comparison between theory and experiment is reasonably good for frequencies up through the resonant frequency. The results tend to diverge at the higher frequencies in the same way as the air tests.

Comparing Figure 9 with Figure 12, it will be seen that water has a significant effect in lowering the cable force. For absolute values of force, the difference in spring constant between air and water must be considered.

c. Segmented Cable Tests in Water

Forced oscillation tests were performed on segmented cables consisting of stranded steel in the upper portion and nylon in the lower portion. Two basic configurations were studied; namely, system No. 2 consisting of 34.5 feet of 1/4-inch nylon joined to 36.5 feet of 3/16-inch steel cable, and system No. 3 consisting of 6 feet of 1/4-inch nylon joined to the bottom of 62 feet of 3/32-inch steel cable. During testing of this latter configuration, a

snap condition was experienced which invalidated using the models presented in this paper. A complete discussion of the results for this specimen is given in [7]. In testing specimen No. 2, the displacement amplitude was one inch to preclude a snap condition. Typical oscillograph traces of the force at the top and bottom of the cable are shown in Figure 13.

Figure 14 shows the comparison between experimental and the theoretical force at the top and bottom of the cable using the distribution mass Voigt Model No. 1. The results were non-dimensionalized based on a measured natural frequency of 1.05 Hz. As the case of pure nylon cables, the comparison is good up through resonance. At higher frequencies, there is a difference which is believed to be caused primarily by the nylon characteristics. As mentioned previously, the nylon stiffness and damping appear to be sensitive to frequency in the high-frequency range. Actually, if the frequency had been increased to cover the second resonant frequency, the cable force at the top is predicted to be somewhat higher than at the first resonant frequency. This is illustrated in [2]. At resonance the cable force is a maximum at the top of the cable, but in the anti-resonance range, the force is higher at the bottom of the cable than at the top. This can be seen both by theory and experiment from Figure 14. Therefore at the higher "modes," the location of maximum cable force can occur anywhere along the cable length, depending on the forcing frequency.

CONCLUSIONS

Based on the experimental and theoretical results, the following conclusions are made.

1. The force response of nylon rope in air for small elongation is fairly linear. The distributed mass Voigt model, which is based on linear theory, yields good predictions up through resonance. At high frequencies, the dimensionless force $\frac{P}{K_o x_o}$ is dependent on excitation amplitude, whereas the theoretical dimensionless force is not. Better agreement in the high-frequency range can be obtained by a three-parameter viscoelastic Model No. 2 with stiffness and internal damping dependent on forcing frequency. The apparent spring constant computed from the natural frequency must be used in preference to the static spring constant.

2. The internal damping measured by a logarithmic decrement approach can be applied to forced oscillation problems with good accuracy. The damping in 1/4-inch nylon rope tested is significant viz $\tau_{ne} = .158$.

3 Water damping has a significant effect on reducing the cable force in the vicinity of resonance. At low frequency, damping appears to actually increase the force slightly. The approximate linear damping coefficient for the payload obtained

from velocity square damping based on equivalence of frictional energy yields results from the distributed mass Voigt Model No. 1, which compare well with experiment. The drag coefficients were based on steady-flow conditions in a range practically insensitive to Reynolds number.

4. The apparent spring constant of nylon braided rope is significantly lower in water than in air. A factor as high as two was computed based on the change in natural frequency between air and water.

5. The distributed mass Voigt Model No. 1 for segmented cables yields good comparisons with experiments in water over the fundamental mode. The experiments verified the theoretical predictions that the force is a maximum at the top of the cable up through the first resonance frequency. The force is a maximum at the bottom of the cable in the vicinity of anti-resonance. This indicates that the location of maximum stress in the cable must be examined closely, since it can occur anywhere along the length of the cable, depending on the forcing frequency.

6. The effect of the virtual mass of water can be accounted for by lumping it with the payload mass.

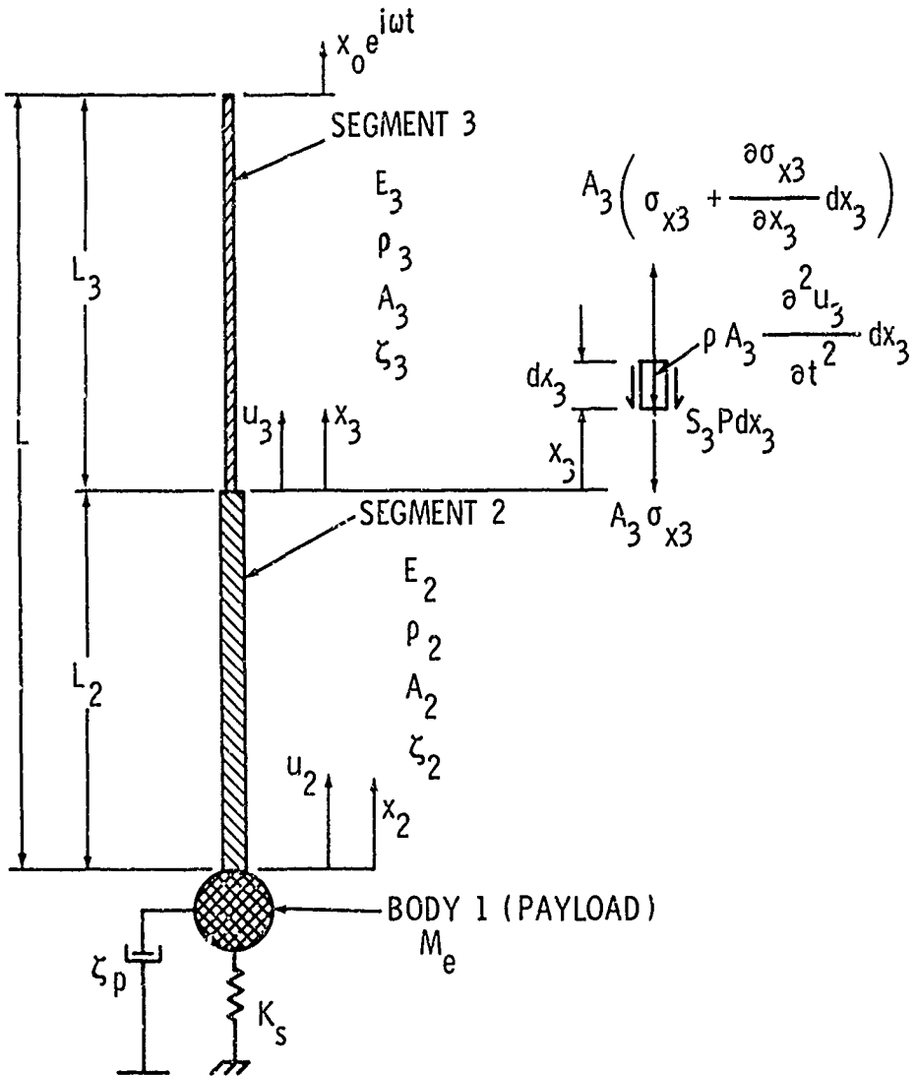

FIG. 1 TWO MATERIAL CABLE SYSTEM

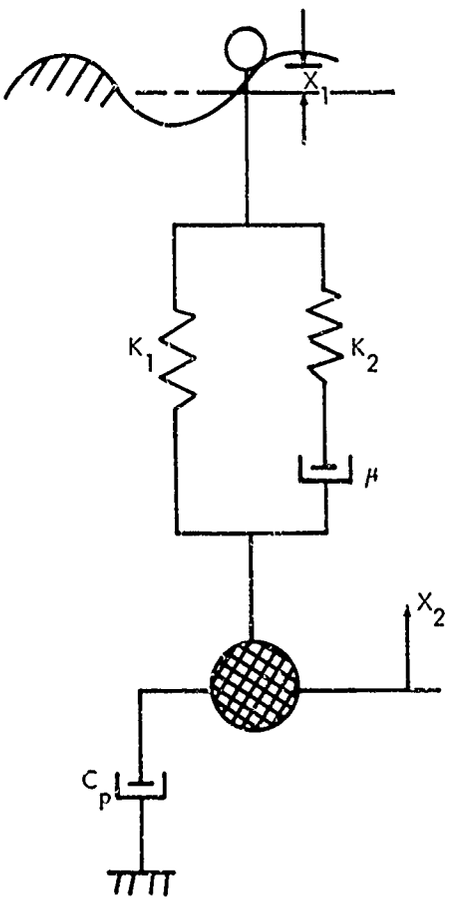

FIG. 2 THREE PARAMETER VISCOELASTIC CABLE MODEL WITH ATTACHED PAYLOAD

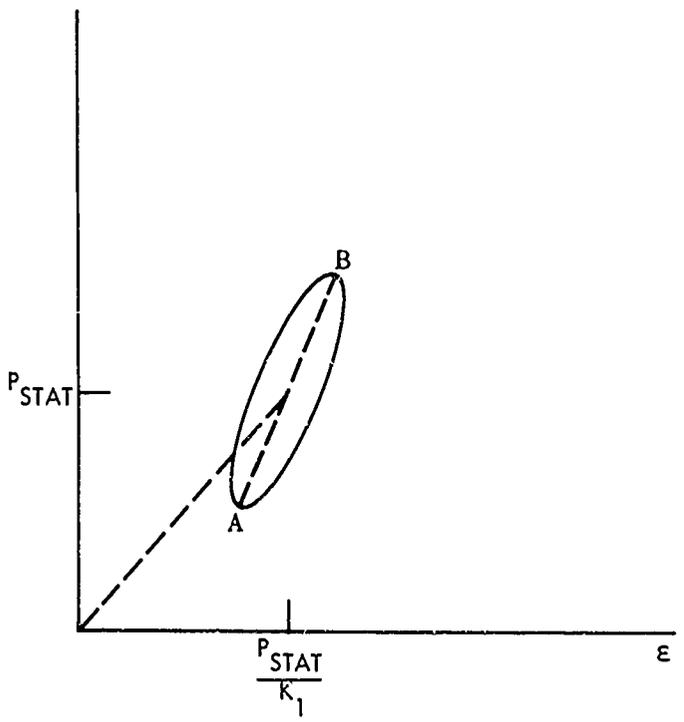

FIG. 3 HYSTERESIS LOOP FOR HARMONIC CYCLING OF THE 3-PARAMETER MODEL

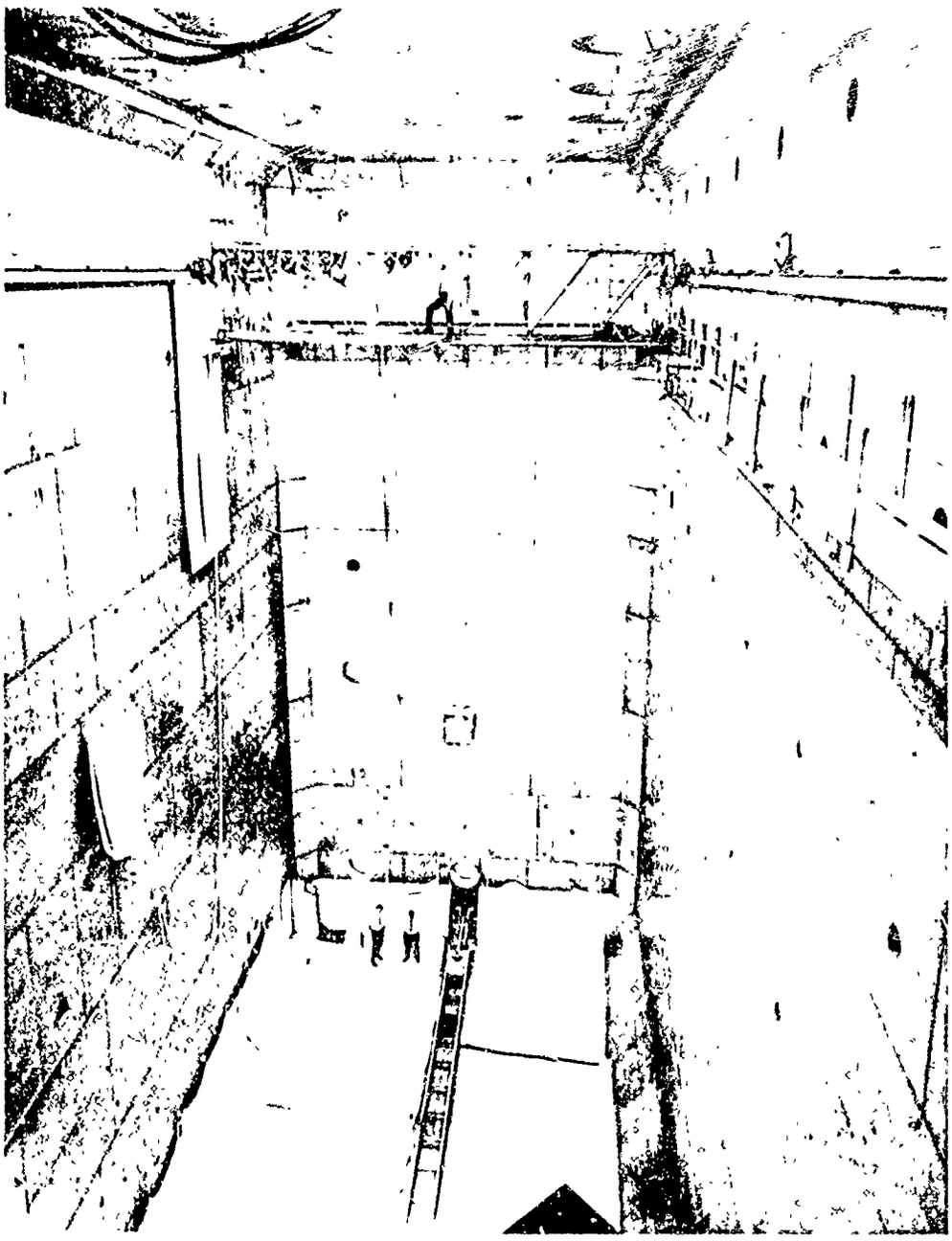

WATER TANK - 100 FEET LONG, 75 FEET DEEP, 35 FEET WIDE
WATER DEPTH - MAXIMUM OF 65 FEET
CONSTRUCTION - STAINLESS STEEL LINED TANK, SUPPORTED BY REINFORCED CONCRETE

FIG. 4 INTERIOR OF HYDRO BALLISTICS FACILITY

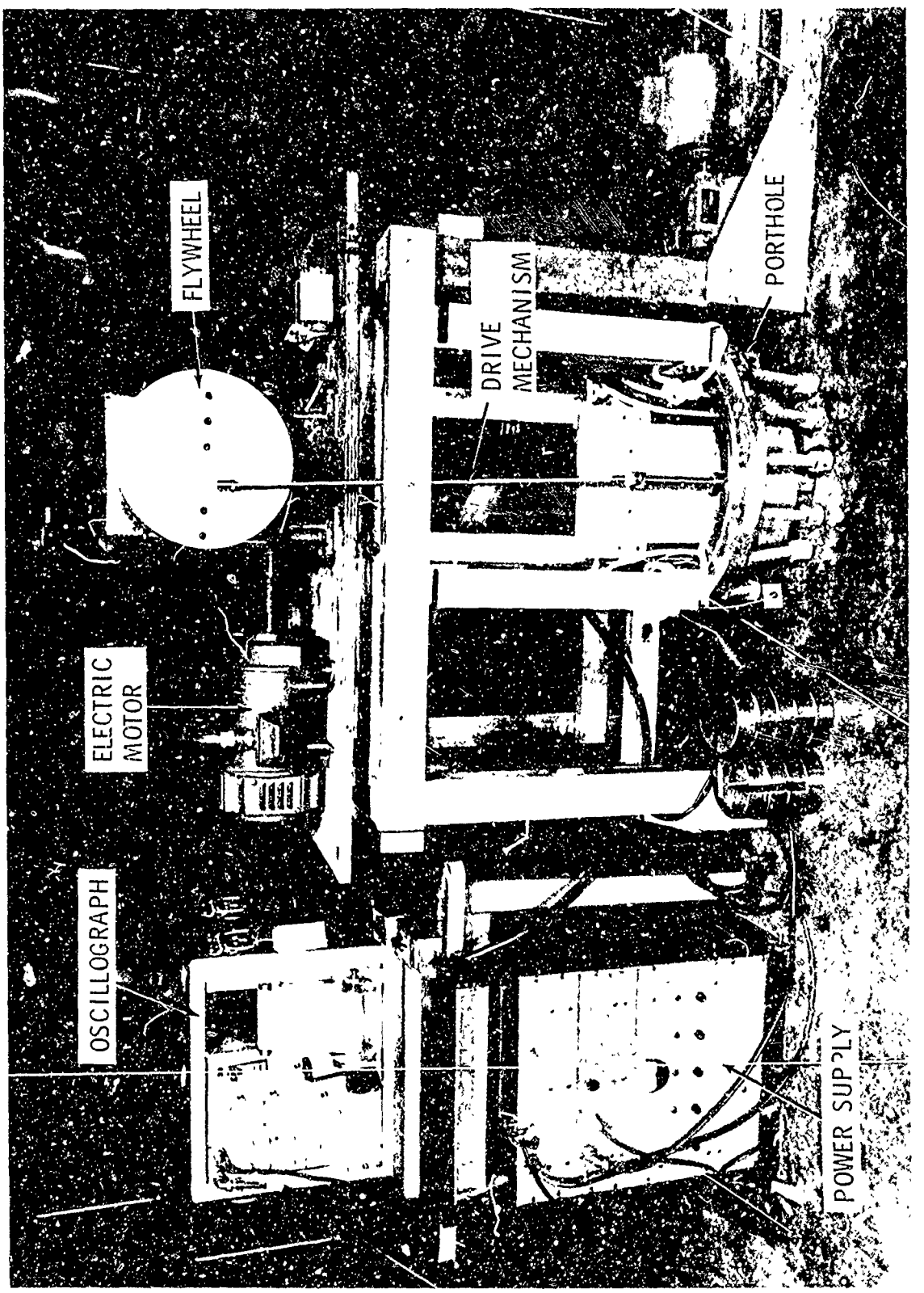

FIG. 5 TEST APPARATUS

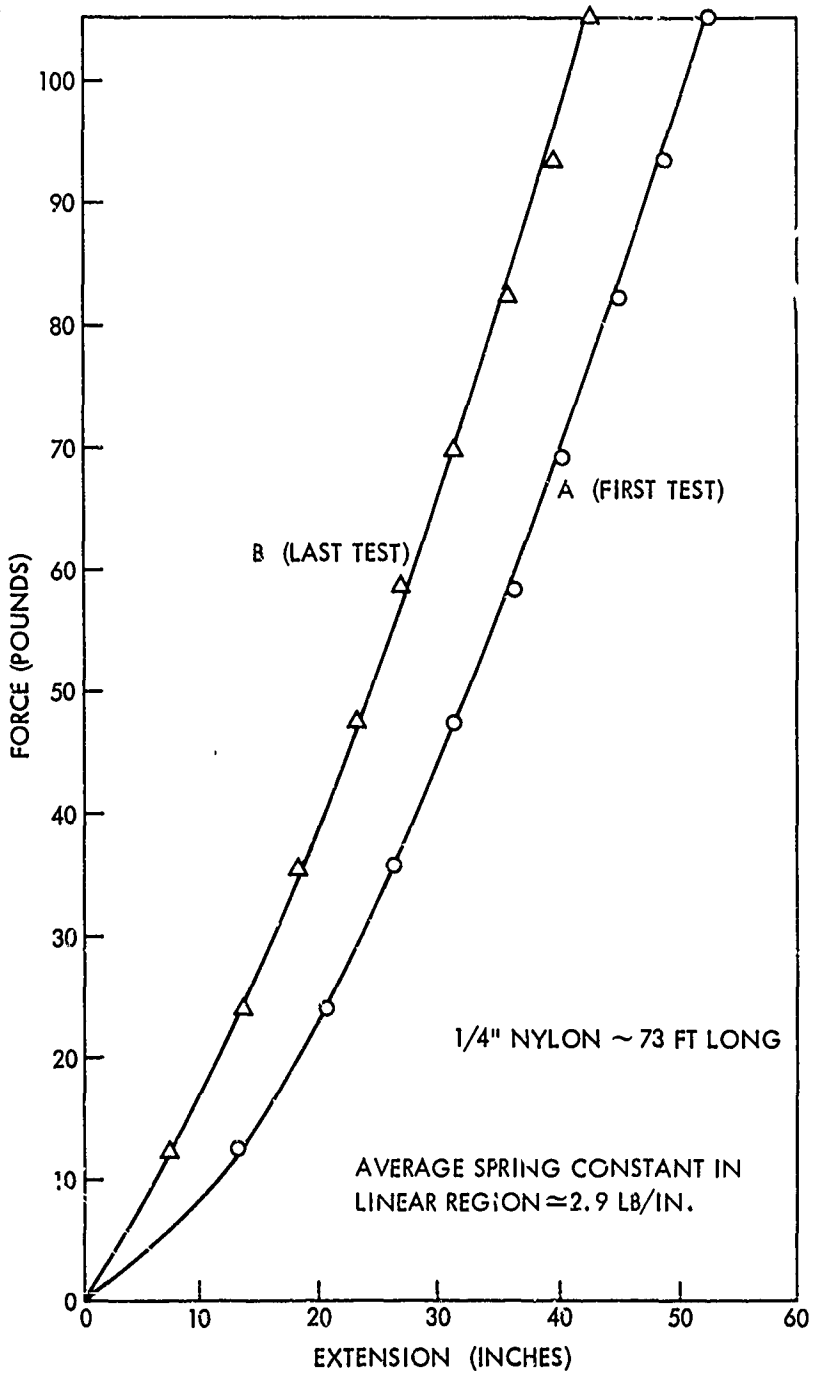

FIG. 6 EXPERIMENTAL FORCE - EXTENSION DATA FOR 1/4 INCH NYLON ROPE

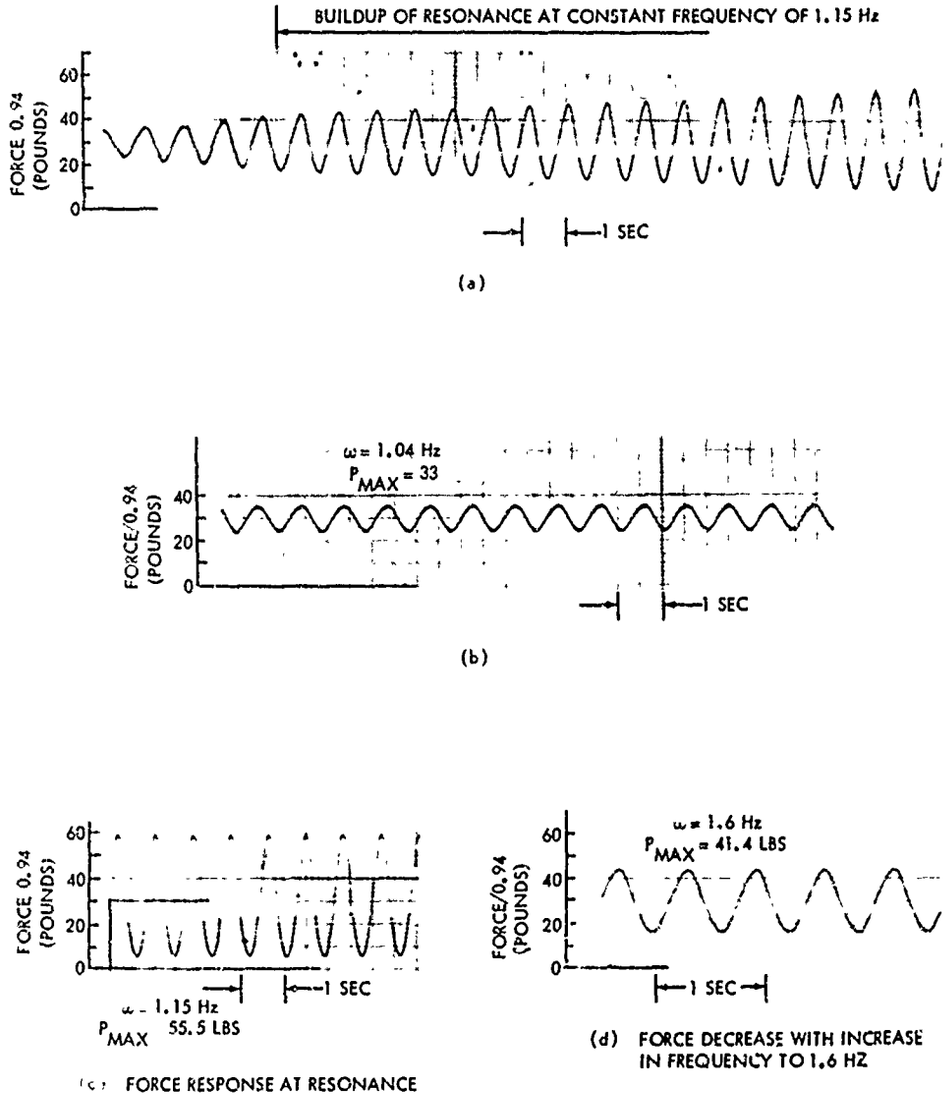

FIG. 7 EXPERIMENTAL FORCE RESPONSE AT TOP OF 1/4 INCH NYLON IN AIR (SYSTEM NO. 1) AT VARIOUS FORCING FREQUENCIES (X_o = 1")

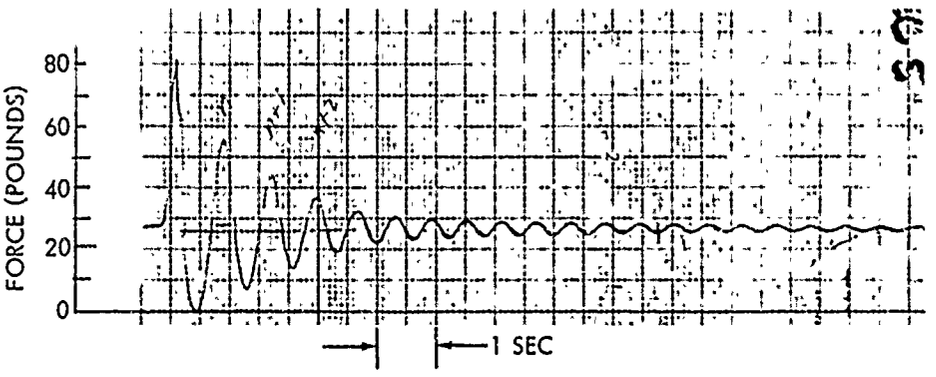

FIG. 8 FREE OSCILLATION RESPONSE OF 1/4" NYLON ROPE IN AIR

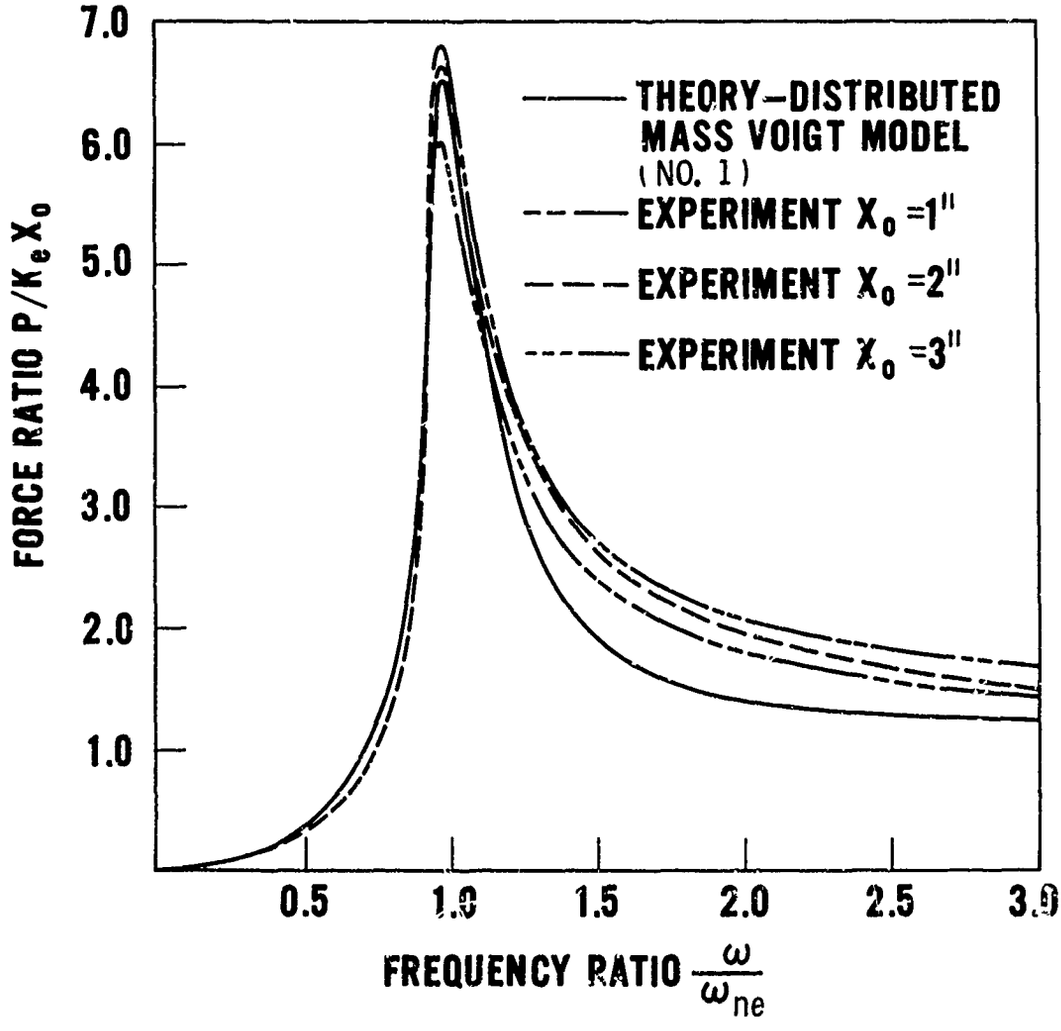

FIG. 9 DIMENSIONLESS FORCE AT TOP OF CABLE (SYSTEM NO. 1) VERSUS FREQUENCY RATIO SHOWING COMPARISON OF EXPERIMENTAL AIR TESTS WITH ANALYTICAL MODEL (NO. 1).

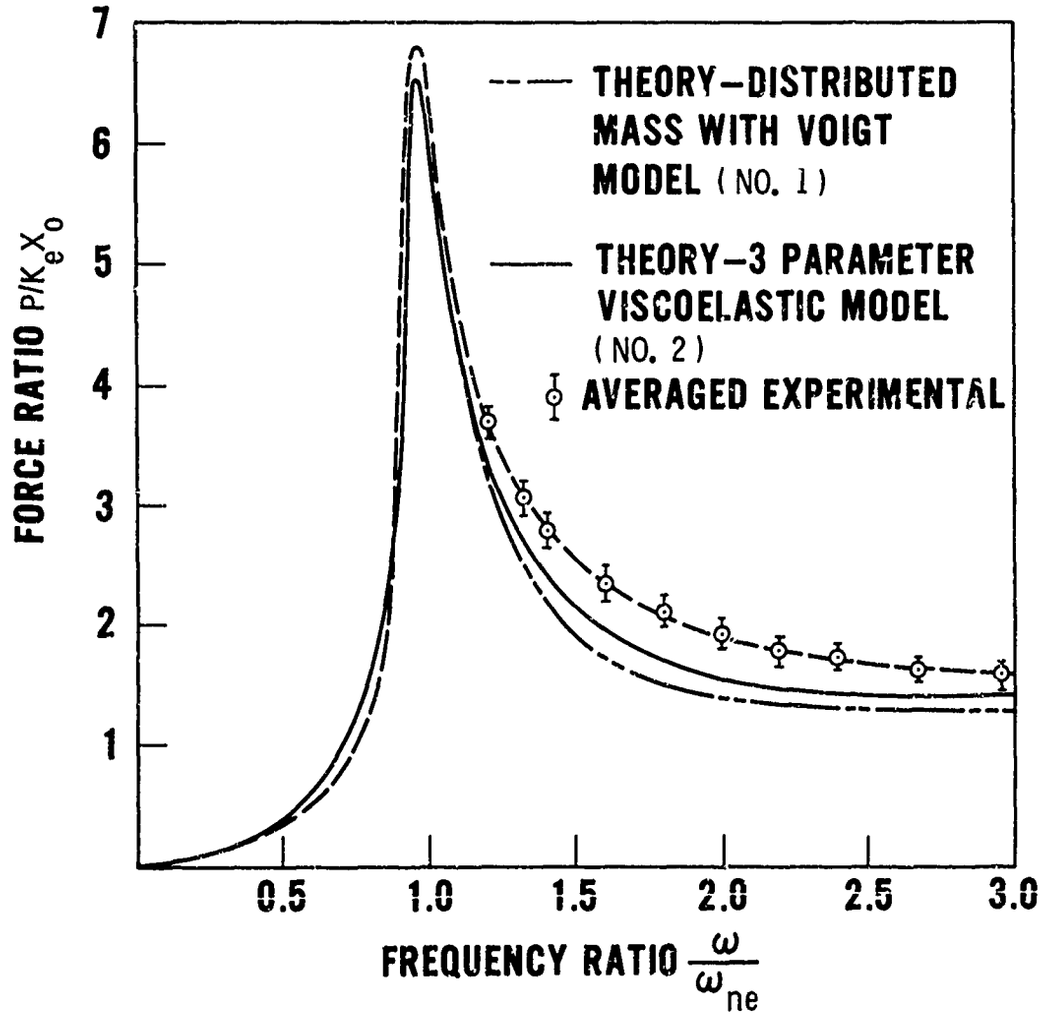

FIG. 10 DIMENSIONLESS FORCE AT TOP OF CABLE VERSUS FREQUENCY RATIO SHOWING COMPARISON OF EXPERIMENTAL AIR TESTS WITH ANALYTICAL MODELS (NO. 1 AND 2).

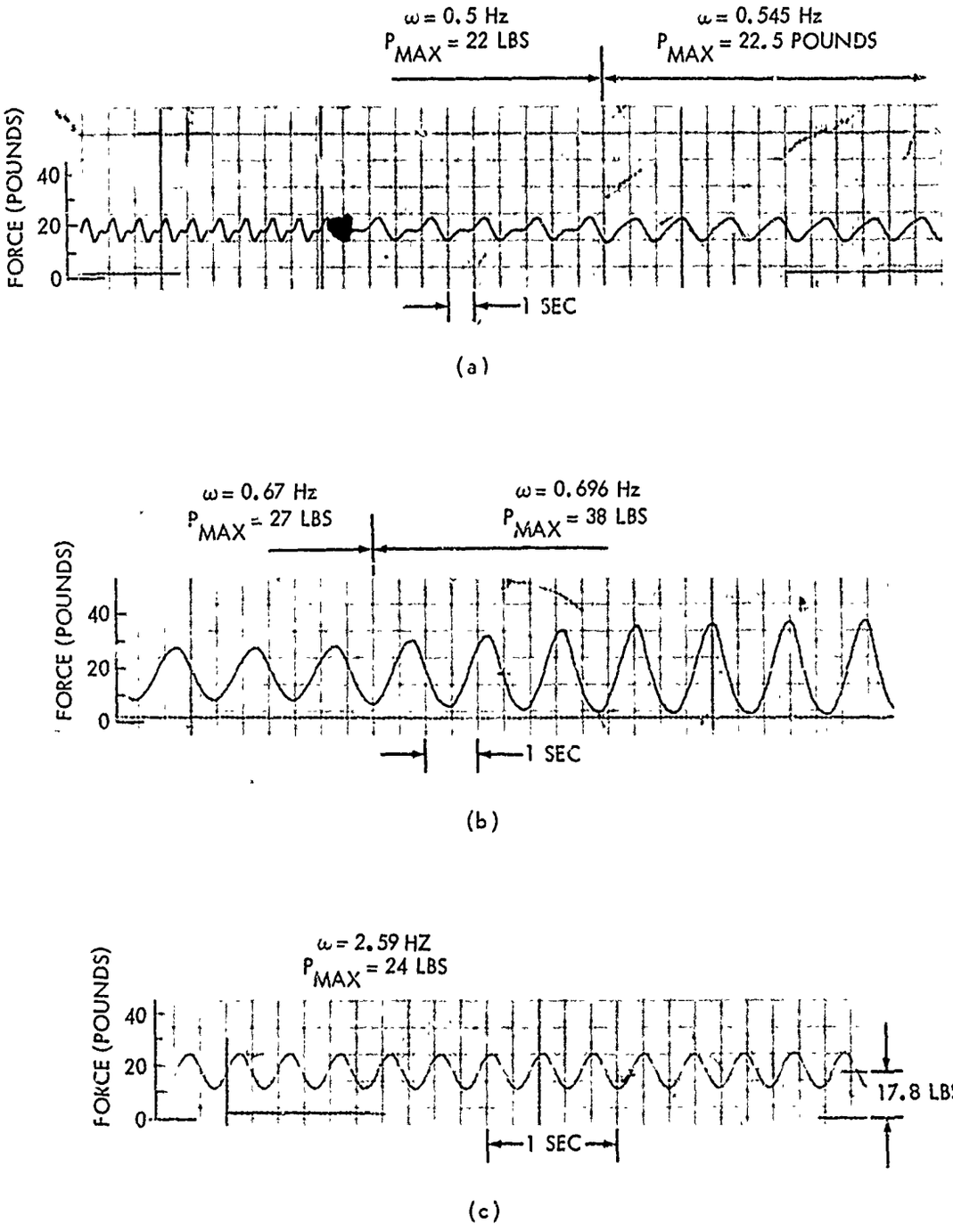

FIG. 11 EXPERIMENTAL FORCE RESPONSE AT TOP OF 1/4" NYLON ROPE IN WATER (SYSTEM NO. 1) AT VARIOUS FORCING FREQUENCIES (X_o=3").

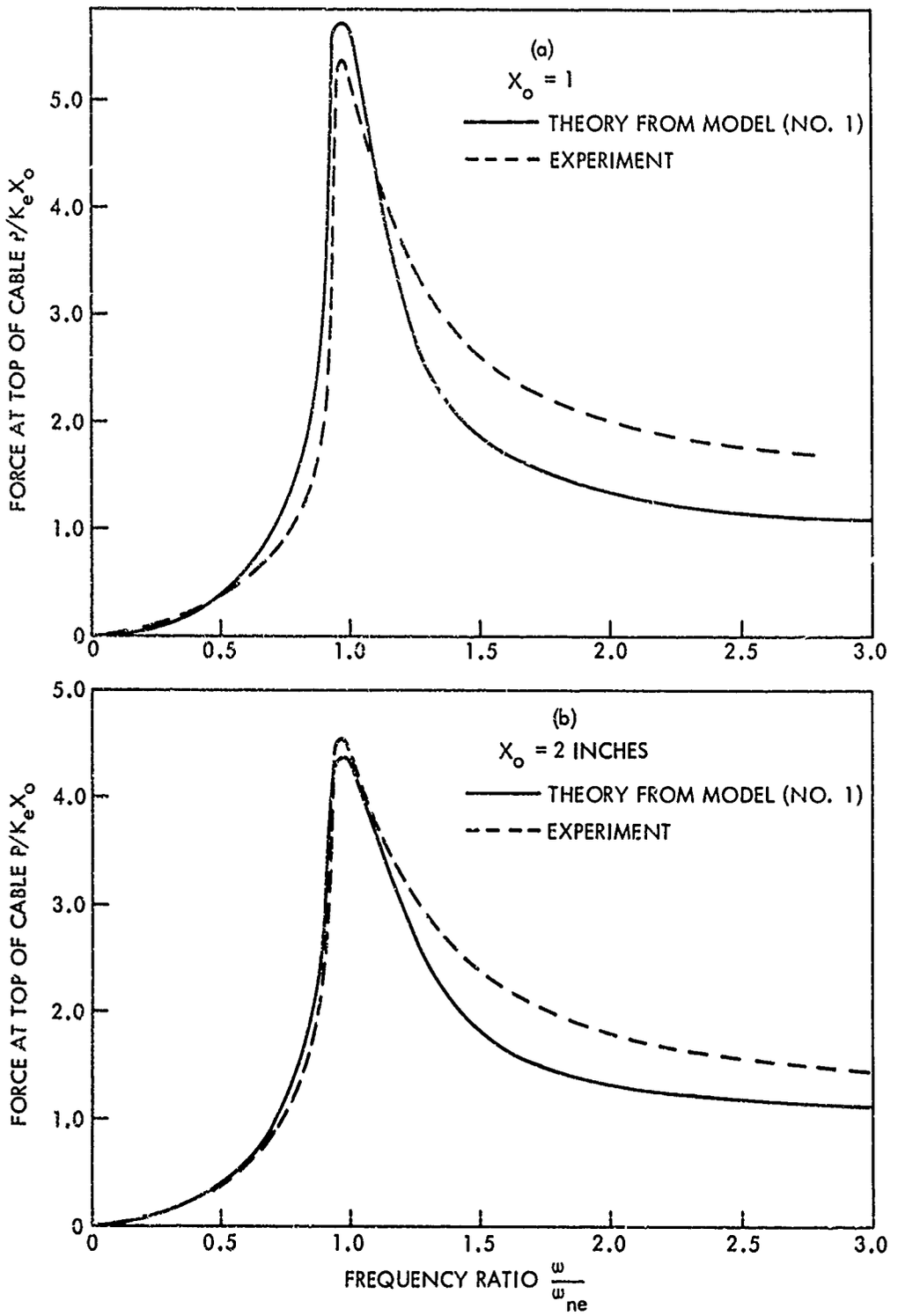

FIG. 12 DIMENSIONLESS FORCE AT TOP OF CABLE VERSUS FREQUENCY RATIO SHOWING COMPARISON OF EXPERIMENTAL WATER TESTS WITH ANALYTICAL MODEL (NO. 1).

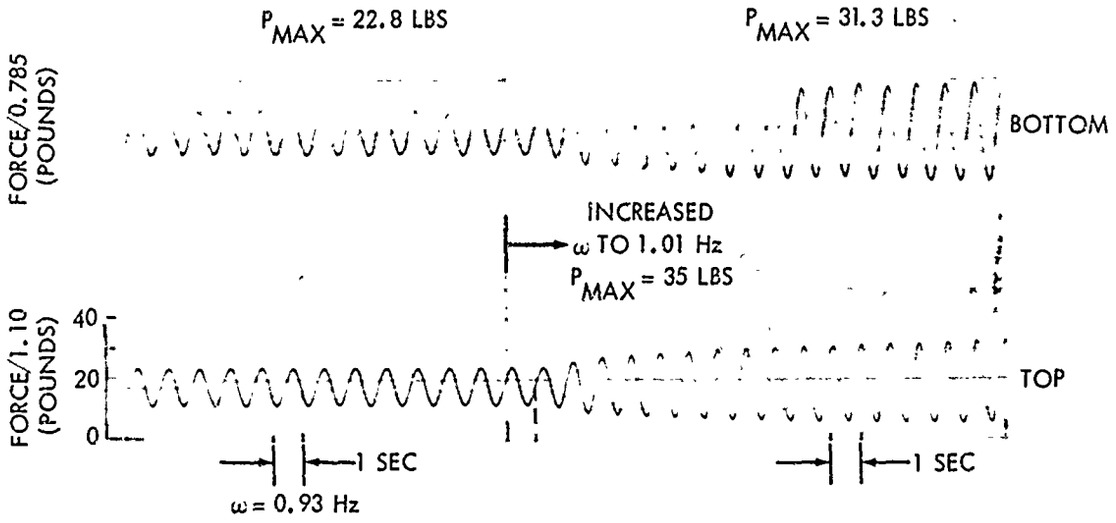

FIG. 13 EXPERIMENTIAL FORCE RESPONSE IN SEGMENTED CABLE (SYSTEM NO. 2) IN WATER AT RESONANCE (X_o = 1")

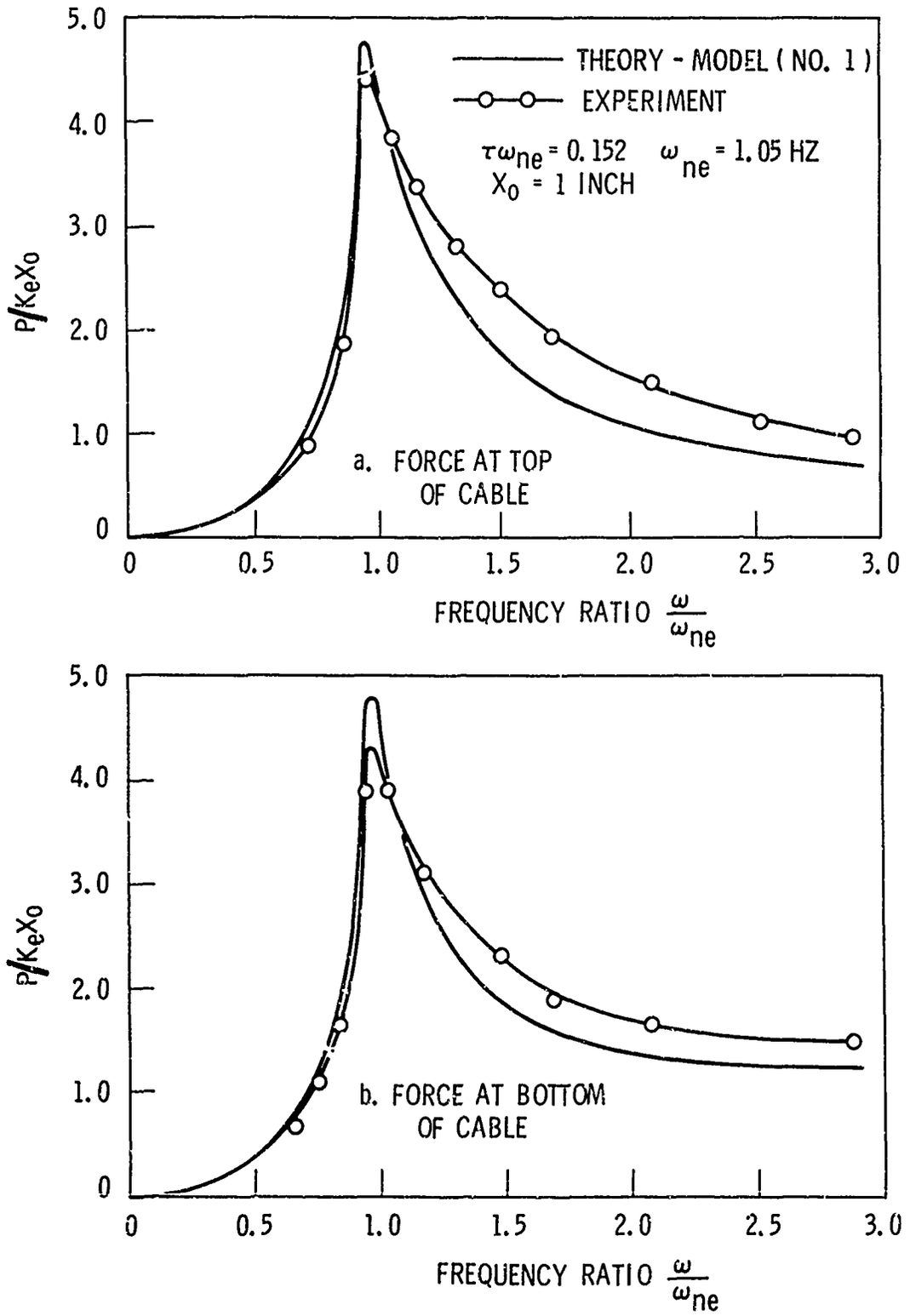

FIG. 14 DIMENSIONLESS FORCE AT TOP AND BOTTOM OF SYSTEM NO. 2 VERSUS FREQUENCY RATIO SHOWING COMPARISON OF EXPERIMENT WITH ANALYTICAL MODEL (NO. 1)

APPENDIX A

APPROXIMATE DAMPING COEFFICIENT FOR NONLINEAR DAMPING

In the previous analysis, the external damping of the payload mass due to fluid viscosity was considered to be linearly proportional to the velocity. Data on various shaped bodies show the drag force in steady flow to be proportional to the velocity squared. In order to use these data, an effective linear damping coefficient was computed by equating the energy dissipated for linear damping to that dissipated for damping proportional to velocity squared. Following this approach, the total energy dissipated for linear damping over a full period of vibration "T" is

$$W = \int_o^T C_p \left(\frac{\partial u_2}{\partial t}\right)^2_{X_2 = 0} dt \qquad \text{(A-1)}$$

For a displacement of the form

$$u_2 \ (o, t) = U_{max} \sin (\omega t - \Phi) \qquad \text{(A-2)}$$

integration of equation (A-1) yields

$$W = \pi \ C_p \ U_{max}{}^2 \ \omega \qquad \text{(A-3)}$$

The total energy dissipated for velocity square damping is

$$W = \frac{\rho \ C_{DP} \ A_p}{2} \int_o^T \left(\frac{\partial u_2}{\partial t}\right)^2 \left|\left(\frac{\partial u_2}{\partial t}\right)\right| dt \qquad \text{(A-4)}$$

where C_{DP} is the drag coefficient. For a sphere, C_{DP} is fairly constant at .5 in the range of Reynolds number of 500 to 5 x 10. Again, utilizing equation (A-2) and integrating equation (A-4), we obtain

$$W = \frac{4}{3} \rho \ C_{DP} \ A_p \ U_{max}{}^3 \ \omega^2 \qquad \text{(A-5)}$$

Equating energies from equation (A-3) and equation (A-5) we obtain

$$C_p = \frac{4}{3\pi} \rho \ C_{DP} \ A_p \ U_{max} \ \omega \qquad \text{(A-6)}$$

Since C_p depends on U_{max}, an iteration technique is used where C_p is assumed and U_{max} computed. The assumed value of C_p is then compared to the calculated value using equation (A-6).

The average damping coefficient $(f\mu)_{aver}$ was computed in a similar manner. The energy dissipated for an element of cable length dx assuming linear damping is

$$\omega = f\mu \, dx \int_o^T \left(\frac{\partial u}{\partial t}\right)^2 dt \qquad (A-7)$$

The energy dissipated over dx for velocity square damping is

$$\omega = \frac{\pi}{2} d \rho C_{DC} \, dx \int_o^T \left(\frac{\partial u}{\partial t}\right)^2 \left|\frac{\partial u}{\partial t}\right| dt \qquad (A-8)$$

Where C_{DC} is obtained from [3] and is defined by $C_{DC} = \frac{F}{\frac{\pi}{2} d \rho V^2}$

Over the first mode of vibration it is reasonable to assume a linear variation of displacement from top to bottom as follows:

$$u = \left[U_{max} - (U_{max} - x_o) \frac{x}{L}\right] \sin (wt - \phi) \qquad (A-9)$$

Using this and equating energies from equations (A-7) and (A-8) we obtain

$$(f\mu)_{aver} = \frac{4}{3} \rho C_{DC} \omega d \left\{ \frac{U_{max}^3 - \frac{3}{2} U_{max}^2 (U_{max} - x_o)}{U_{max}^2 - U_{max} (U_{max} - x_o) + \frac{(U_{max} - x_o)^3}{3}} + \frac{U_{max} (U_{max} - x_o)^2 - .25 (U_{max} - x_o)^3}{U_{max}^2 - U_{max} (U_{max} - x_o) + \frac{(U_{max} - x_o)^3}{3}} \right\}$$

UNCLASSIFIED

Security Classification

DOCUMENT CONTROL DATA - R & D

(Security classification of title, body of abstract and indexing annotation must be entered when the overall report is classified)

1 ORIGINATING ACTIVITY (Corporate author) U S Naval Ordnance Laboratory White Oak, Silver Spring, Maryland 20901	2a. REPORT SECURITY CLASSIFICATION UNCLASSIFIED 2b. GROUP

3 REPORT TITLE

ANALYTICAL AND EXPERIMENTAL STUDY OF THE DYNAMIC RESPONSE OF CABLE SYSTEMS

4 DESCRIPTIVE NOTES (Type of report and inclusive dates)

5 AUTHOR(S) (First name, middle initial, last name)

Jack E. Goeller

6. REPORT DATE	7a. TOTAL NO. OF PAGES	7b. NO. OF REFS
23 February 1970	47	7

8a. CONTRACT OR GRANT NO.	9a. ORIGINATOR'S REPORT NUMBER(S)
b. PROJECT NO.	NOLTR 70-38
c.	9b. OTHER REPORT NO(S) (Any other numbers that may be assigned this report)
d.	

10 DISTRIBUTION STATEMENT

This document has been approved for public release and sale, its distribution is unlimited.

11. SUPPLEMENTARY NOTES	12. SPONSORING MILITARY ACTIVITY

13 ABSTRACT

The dynamic response of steel and nylon cables with a suspended payload in water was investigated analytically and experimentally. Ocean wave motion was simulated at the top of the cables by a sinusoidal displacement function. A generalized distributed mass analytical model including internal and external damping was used to predict cable tone. Experimental results on cables of the order of 70 feet in length and .25 inch diameter compared well with theoretical predictions.

DD FORM 1 NOV 65 1473 (PAGE 1)

S/N 0101-807-6801

UNCLASSIFIED

Security Classification

14 KEY WORDS	LINK A		LINK B		LINK C	
	ROLE	WT	ROLE	WT	ROLE	WT
Cable vibration Response of cables Cable stress						